Inorg. Chem. **2002**, *41*, 6604–6613

Room-Temperature Synthesis and Crystal, Magnetic, and Electronic Structure of the First Silver Copper Oxide

Eva M. Tejada-Rosales,[†] Juan Rodríguez-Carvajal,[‡] Nieves Casañ-Pastor,[†] Pere Alemany,[§] Eliseo Ruiz,[§] M. Salah El-Fallah,[§] Santiago Alvarez,[§] and Pedro Gómez-Romero*[,†]

Institut de Ciència de Materials de Barcelona (CSIC), Campus UAB, E-08193 Bellaterra, Barcelona, Spain, Laboratoire Leon Brillouin, (CEA-CNRS), Centre d'Etudes de Saclay, 91191 Gif sur Yvette Cedex, France, and Departament de Química Inorgànica, Facultat de Química, Universitat de Barcelona, Diagonal 647, E-08028 Barcelona, Spain

Received July 12, 2002

$Ag_2Cu_2O_3$ is the first known silver copper oxide. It was prepared by coprecipitation at room temperature and ambient pressure and shows an increased thermal stability compared with silver oxides. The crystal structure (tetragonal, $a = 5.8862(2)$ Å, $c = 10.6892(4)$ Å, $Z = 4$, $I4_1/amd$) was refined from neutron and X-ray powder diffraction data, and it is related to that of the mineral paramelaconite (Cu_4O_3). In addition to a thorough characterization (chemical and TG analyses, XPS, crystal structure, and electrochemical, magnetic, and transport properties), we have carried out band structure calculations [extended Hückel tight binding (EHTB) and spin polarized density functional (DFT) band calculations] for the title silver copper oxide and for the related paramelaconite structure (Cu(II)–Cu(I) mixed-valence system) with special incidence into the magnetic behavior and coupling constants in these magnetically novel 3-D compounds. This new oxide represents an important precedent in solid state inorganic chemistry but also has potential interest concerning its magnetic, electrochemical, and catalytic properties.

Introduction

Copper and silver belong to the same family, share common features, and readily form alloys in their metallic states. Nevertheless, when it comes to forming ternary compounds, there seems to be a different story. Thus, no mixed silver copper oxide was hitherto known in nature, and none had been previously synthesized. Only a few simple silver copper compounds were known. Among them, halides,[1] sulfides (stromeyerite, AgCuS,[2,3] and jalpaite, Ag_3CuS_2[4]), and a phosphate.[5]

In this respect, the first silver copper oxide known to date, $Ag_2Cu_2O_3$, which was previously communicated by our group[6] and is reported here in full detail, represents an important precedent. Indeed, after the synthesis of this oxide, several attempts have been made in order to prepare new ternary Ag−Cu−O phases, as will be discussed. Furthermore, other more complex silver−copper phases have also been prepared, such as the solid solution $Ag_5Pb_{2-x}Cu_xO_6$ ($0 \geq x \geq 0.5$) which is, to our knowledge, the first quaternary silver copper oxide.[7]

The original thrust for research on silver copper oxides came from the field of cuprate superconducting materials. Many efforts were made to prepare complex silver copper oxides in an attempt to synthesize new high-temperature superconductors similar to the mercury containing phases that still hold record critical temperatures. These efforts aimed at the substitution of toxic lead or mercury by the chemically analogous and safer silver ions.

Among reports published in the literature with this declared objective,[8−10] there have been some research efforts com-

* Corresponding author. E-mail: pedro.gomez@icmab.es. Fax: 34935805729.
[†] Institut de Ciència de Materials de Barcelona.
[‡] Laboratoire Leon Brillouin.
[§] Universitat de Barcelona.

(1) Saito, M.; Tamaki, S. *Solid State Ionics* **1993**, *60*, 237−74.
(2) Frueh, A. J., Jr. *Z. Kristallogr. (A)* **1955**, *106*, 299−307.
(3) Baker, C. L.; Lincoln, F. J.; Johnson, A. W. S. *Acta Crystallogr., Sect. B* **1991**, *47*, 891−899.
(4) Baker, C. L.; Lincoln, F. J.; Johnson, A. W. S. *Aust. J. Chem.* **1992**, *45*, 1441−1449.
(5) Quarton, M.; Oumba, M. T. *Mater. Res. Bull.* **1983**, *18*, 967−974.
(6) Gómez-Romero, P.; Tejada-Rosales, E. M.; Palacín, M. R. *Angew. Chem., Int. Ed.* **1999**, *38*, 524−525; *Angew. Chem.* **1999**, *111*, 544−546.
(7) Tejada-Rosales, E. M.; Oro-Sole, J.; Gómez-Romero, P. *J. Solid State Chem.* **2002**, *163*, 151−157.
(8) Alario-Franco, M. A. *Physica C* **1994**, *231*, 103−108.
(9) Ihara, H.; Tokiwa, K.; Ozawa, H.; Hirabayashi, M.; Matuhata, H.; Negishi, A.; Song, Y. S. *Jpn. J. Appl. Phys.* **1994**, *33*.

10.1021/ic025872b CCC: $22.00
Published on Web 11/15/2002

petently done that, despite failures to isolate the intended silver copper oxides, have led to the isolation of novel and interesting cuprate phases.[8] On the other hand, some groups have claimed the isolation of silver copper oxides with less than adequate analyses, even with diffraction patterns where peaks from metallic silver are cited as evidence for the isolation of new phases.[10] In all these cases, the reported syntheses relied upon the application of high O_2 pressures which were nonetheless insufficient to compensate for the well-known marked instability of silver oxides toward thermal decomposition to yield metallic silver. These precedents made evident the need for alternative strategies and a better understanding of the chemistry of Ag−Cu−O phases.

We have undertaken that challenge from a more basic point of view, by aiming at the preparation of simpler mixed silver copper oxides. Furthermore, our approach has centered on the use of well-known low-temperature soft chemistry syntheses as an alternative to high-O_2 pressure methods in order to avoid the formation of metallic silver. The result has been the isolation of the first silver copper oxide known to date, which has been previously communicated by our group[6] and is reported here in full detail. Specifically, this paper contains an optimized synthetic procedure at room temperature, the refinement of the structure by simultaneous Rietveld analysis of neutron and X-ray data to yield a more precise structural model than that originally communicated, and a thorough characterization of physical−chemical properties of the oxide, including thermal analyses, XPS, electrochemistry, and magnetic and transport properties. In addition to the experimental data and results, theoretical calculations concerning band structure and magnetism have been performed and are also reported here.

Experimental Section

Synthesis. $Cu(NO_3)_2{\cdot}3H_2O$ (0.77 g, 3.2 mmol) (Merck, p.a. 99.5%) and $AgNO_3$ (0.52 g, 3.1 mmol) (Panreac, p.a., 99.98%) as purchased were dissolved in 2 mL of deionized water. The resulting silver−copper solution was added to an aqueous solution of NaOH 3 M (4 mL) with very vigorous stirring (in order to avoid the formation of blue $Cu(OH)_2$), and a dark-green precipitate was formed. This solid precursor of unknown structure (apparently containing amorphous $Cu(OH)_2$ and Ag_2O) was left stirring in the solution for at least 6 h at room temperature. During this period and if an inert atmosphere is not used, it has been found advisable to add some water (ca. 40 mL) to decrease the alkalinity of the solution in order to avoid the formation of carbonates from ambient CO_2. The dark green powder turned spontaneously into the final black product, $Ag_2Cu_2O_3$, which was vacuum-filtered and washed with water until reaching a neutral pH of the filtrate. The solid precursor could also be mildly heated in air at temperatures between 60 and 170 °C for 6 h to yield the oxide $Ag_2Cu_2O_3$. In both cases (aging at room temperature or mild heating), the oxide was obtained quantitatively.

Characterization. Atomic absorption spectroscopy was carried out with a Unicam PU 9200X instrument using deuterium corrections. For thermal analyses, a Perkin-Elmer TGA 7 was used. All the experiments were carried out under a controlled dynamic atmosphere, heating at 2 °C/min. For the determination of oxygen contents, an atmosphere of Ar/H_2 (5% v/v H_2) was used. Microanalysis and electron diffraction were carried out in an analytical transmission electron microscope JEOL-JEM-1210. For microanalysis, a minimum of 20 microcrystals per batch were analyzed. The powder X-ray data were collected in a Rigaku X-ray powder diffractometer "Rotaflex" Ru-200B, $10° < 2\theta < 90°$, step 0.02°, Cu Kα radiation ($\lambda = 1.5418$ Å). A high-resolution powder neutron diffraction pattern was collected using the diffractometer 3T2 at the reactor ORPHEE of the Laboratoire Leon Brillouin. This diffractometer has a (335)-Ge monochromator at a takeoff angle of about 90°, providing neutrons of wavelength 1.22 Å coming from a primary collimator of 10′ divergence. Soller collimators of 8′ divergence in front of the 20 detectors improve the final resolution. The maximum 2θ recorded angle is 125.45°, providing a maximum momentum transfer of $Q_{max} = 9.1$ Å^{-1}. The total number of independent reflections was 175. X-ray and neutron diffraction data were simultaneously used for the refinement of the crystal structure by the Rietveld method using program FULLPROF.[11] XPS experiments were performed on an ESCALAB 200 spectrometer operating in the constant pass energy mode (50 eV) and using unmonochromated Mg K radiation (1253.6 eV) as the excitation source. The base pressure in the analysis chamber was close to 10^{-10} mbar. Energy resolution of the instrument was measured at the full-width at half-maximum (1.5 eV) of the $Ag3d_{5/2}$ signal for a silver foil cleaned by ion sputtering with argon. The samples, as pressed pellets, were previously degassed up to 10^{-10} mbar at room temperature for 24 h. No spectral changes were observed during the spectra acquisition (samples are stable toward X-ray irradiation). Electrochemical studies were carried out with a potenciostat/galvanostat EG&G PAR 273A or 263A. One-compartment cells with three electrodes were used. Platinum coil was used as counter electrode, and gold foil was used as pseudo-reference-electrode. Working electrodes were prepared as pellets by pressing the oxide powders. No conducting matrix was added because the conductivity of the oxide was high enough to allow good electrical flow. Electrical contacts were made by means of colloidal silver paste. An HP 4192ALF impedance analyzer 5 Hz-13 MHz or a Solartron Schlumberger 1250 frequency response analyzer with a Solartron Schlumberger 1286 electrochemical interface was used for the measurement of transport properties. The sample was prepared as pellets, using silver paste as contact and using gold electrodes. Magnetic susceptibility was measured under different constant magnetic fields in the temperature range 5−300 K by means of a Quantum Design SQUID magnetometer using approximately 20 mg of powdered sample.

Computational Details. The qualitative discussion of the electronic band structures of Cu_4O_3 and $Ag_2Cu_2O_3$ is based on extended Hückel[12,13] tight-binding[14,15] calculations, with the modified Wolfsberg−Helmholz formula[16] for the evaluation of the off-diagonal elements of the Hamiltonian matrix, as implemented in the CASSANDRA[17] code, and the band dispersion and DOS diagrams were generated with the viewkel routine of the YAeHMOP[18] package. The ionization potentials adopted in these calculations are those reported by Vela and Gázquez.[19] For extended

(10) El-Hofy, M. I.; Donia, A. M.; Abou-Sekkina, M. M. *J. Mater. Sci. Technol.* **1999**, *15*, 87−90.

(11) Rodriguez-Carvajal, J. *FULLPROF*, 1.5 April 2000; Laboratoire Leon Brillouin (CEA-CNRS): France, 2000.

(12) Hoffmann, R.; Lipscomb, W. N. *J. Chem. Phys.* **1962**, *36*, 2179.

(13) Hoffmann, R. *J. Chem. Phys.* **1963**, *39*, 1397.

(14) Whangbo, M.-H.; Hoffmann, R. *J. Am. Chem. Soc.* **1978**, *100*, 6093.

(15) Whangbo, M.-H.; Hoffmann, R.; Woodward, R. B. *Proc. R. Soc. London, Ser. A* **1979**, *366*, 23.

(16) Ammeter, J. H.; Bürgi, H.-B.; Thibeault, J. C.; Hoffmann, R. *J. Am. Chem. Soc.* **1978**, *100*, 3686.

(17) Llunell, M.; Alemany, P.; Ruiz, E. *Cassandra*; Universitat de Barcelona: Barcelona, 1999.

systems, numerical integrations over the irreducible wedge of the Brillouin zone have been performed using a 90 *k*-point mesh. The evaluation of the energies of the different spin states was obtained via density functional calculations using the CRYSTAL-98 package[20] with the B3LYP combination of exchange and correlation functionals and a triple-ζ quality basis set[21] to evaluate the relative energies of the different spin arrangements for the four unpaired electrons in the unit cell. For the calculation of the Coulomb and exchange integrals, tolerance factors[22] of 7, 7, 7, 7, and 14 were used. The convergence criterion for the energy was set at 10^{-7} au. Integration of *k*-dependent magnitudes in the reciprocal space was carried out using a mesh of 46 *k*-points for the ferromagnetic state (abbreviated F, with neighboring spins ferromagnetically ordered both within and between the chains) and one of the low spin states (A, with ferromagnetic ordering within and antiferromagnetic coupling between the chains) and of 68 *k*-points for another low spin state (A′, in which the Cu^{II} ions are antiferromagnetically coupled along the chains).

Results and Discussion

Room-Temperature Synthesis. The synthesis of the title oxide takes place by alkaline coprecipitation of a mixed solution of silver and copper ions to yield a intermediate solid which, upon aging, leads to crystalline $Ag_2Cu_2O_3$ in quantitative yields. This reaction is remarkable in that it represents a very simple alternative to high-temperature, high-pressure procedures conventionally used to overcome the instability of silver oxides and other noble transition oxides toward thermal decomposition to yield the corresponding metals. It should be noted that, although the concept reaction and the procedure are simple, some complications could lead to the formation of impurities. Thus, the synthetic procedure reported here has been optimized to avoid the formation of copper hydroxide or carbonates during precipitation and aging.

Chemical Analyses. The analyses of bulk powder samples indicate the formula $Ag_2Cu_2O_3$ [Anal. Found: Ag 53.4%, Cu 33% (by atomic absorption); O 12.3% by TGA in Ar/H_2 dynamic atmosphere. Calcd for $Ag_2Cu_2O_3$: Ag 55.2%, Cu 32.5%, O 12.3%]. Moreover, microanalyses were carried out on a statistically significant number of crystals for a given sample (see Experimental Section) by energy dispersive X-ray analyses (EDX) in the analytical transmission electron microscope. They show the presence of Ag and Cu in a constant ratio in 99% of the microcrystals analyzed, confirming the isolation of a pure homogeneous phase. Furthermore, XPS analyses also show a homogeneous clean phase with peaks unambiguously assigned to Ag(I) and Cu(II) (see later).

Thermal Stability. The new compound was analyzed by TGA and DTA. The analyses were carried out in different dynamic atmospheres: Ar, air, oxygen, and Ar/H_2 (5% v/v). Some of those results are shown in Figure 1. $Ag_2Cu_2O_3$ suffers a single step decomposition to yield metallic Ag and Cu (under Ar or Ar/H_2 atmospheres), or Ag and CuO under air or oxygen. The decomposition of $Ag_2Cu_2O_3$ takes place at 260 °C in the case of Ar/H_2, at 340 °C in Ar, at 354 °C in air, and at 368 °C in oxygen (temperatures corresponding to the inflection points of the weight losses). Furthermore, we have observed a correlation between synthetic temperature and thermal stability of $Ag_2Cu_2O_3$.[23] Although the reasons for this correlation are not yet clear, the higher the synthesis temperature the greater the thermal stability of the sample obtained. All the results obtained show a remarkable stabilization of the title oxide toward thermal decomposition in comparison with silver oxide, which decomposes at only 100 °C under Ar/H_2.

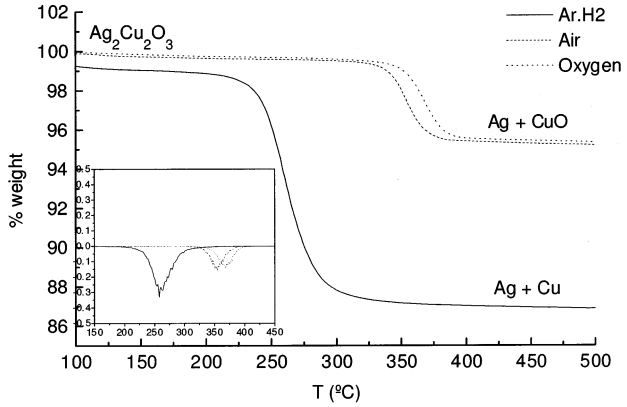

Figure 1. Thermogravimetric analyses of $Ag_2Cu_2O_3$ under the indicated controlled dynamic atmosphere. Heating rate: 2 °C/min.

The DTA in argon shows an endothermic process taking place at 341 °C which corresponds to the same decomposition process detected by TGA mentioned earlier.

X-ray Photoelectron Spectroscopy. The sample was analyzed by XPS as synthesized after degassing in the analysis chamber for 24 h at room temperature. Carbon or other contaminant or segregated elements were not present at the surface, as only signals due to Cu, Ag, and O were observed. Main signals due to copper (Cu2p and CuLMM lines) show all the same features (energy positions, shake up satellites, and Auger parameter value) observed for Cu(II) in CuO bulk samples,[24] while signals due to silver (Ag3d and AgMVV lines) are typical for Ag(I) in silver oxides (Ag_2O and AgO).[25,26] Finally, in the spectral zone for O1s, two peaks are observed: the major one, located at 529.5 eV (Binding Energy) is due to O^{2-} species as those observed in CuO and Ag_2O; the minor one, a shoulder located at around 531 eV, is likely due to OH^- species.[27]

Crystal Structure: Powder X-ray, Neutron, and Electron Diffraction. Preliminary X-ray powder diffraction patterns[6] were indexed in the tetragonal system (a =

(18) Landrum, G. *YAeHMOP− Yet Another Extended Hückel Molecular Orbital Package*, 1.1 Cornell University: Ithaca, NY, 1995.
(19) Vela, A.; Gázquez, J. L. *J. Phys. Chem.* **1988**, *92*, 5688.
(20) Saunders, V. R.; Dovesi, R.; Roetti, C.; Causà, M.; Harrison, N. M.; Orlando, R.; Zicovich-Wilson, C. M. *CRYSTAL98*; University of Torino: Torino, Italy, 1998.
(21) Ruiz, E.; Alvarez, S.; Alemany, P.; Evarestov, R. A. *Phys. Rev. B* **1997**, *56*, 7189.
(22) Pisani, C.; Dovesi, R.; Roetti, C. *Hartree−Fock Ab Initio Treatment of Crystalline Solids*; Springer-Verlag: Berlin, 1988.
(23) Tejada-Rosales, E. M.; Palacín, M. R.; Gómez-Romero, P. *Bol. Soc. Esp. Ceram. Vidrio* **2000**, *39*, 209−212.
(24) Wagner, C. D. *Auger and X-ray Photoelectron Spectroscopy*; Wagner, C. D., Ed.; Wiley: New York, 1990; Vol. 1, pp 608 and references therein.
(25) Gaarenstroom, S. W.; Winograd, N. *J. Chem. Phys.* **1977**, *67*, 3500.
(26) Bao, X.; Muhler, M.; Schedel-Niedrig, T.; Schlögl, R. *Phys. Rev. B* **1996**, *54*, 2249.
(27) González-Elipe, A. R.; Espinós, J. P.; Fernández, A.; Munuera, G. *Appl. Surf. Sci.* **1990**, *45*, 103.

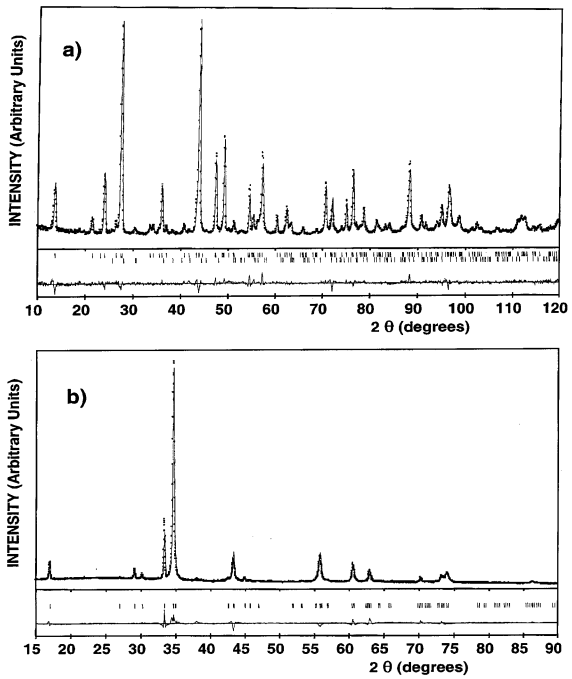

Figure 2. Neutron (a) and X-ray (b) Rietveld refinement for the $Ag_2Cu_2O_3$ structure. Dots correspond to experimental data, the continuous lines are the calculated profiles, and the bottom line is the difference between both. Small vertical lines mark the position of allowed Bragg reflections for $Ag_2Cu_2O_3$ (top) and CuO (bottom).

5.8857(3) Å, $c = 10.6868(7)$ Å), whereas electron diffraction studies[23] allowed the reconstruction of the reciprocal lattice and the identification of systematic absences, which were unambiguously consistent with space group $I4_1/amd$. Those results were later confirmed by a single-crystal X-ray diffraction study.[28,29]

The collection of neutron diffraction data was necessary to yield a more precise structural model with reliable coordination geometries. This technique provides the best way to find precise positional and thermal parameters for light atoms such as oxygen in structures containing heavy metals such as the one at hand and in that way leads to the determination of reliable coordination geometries. Thus, neutron powder data were collected, and the structure of $Ag_2Cu_2O_3$ has been now refined using the Rietveld method, by simultaneous analysis of neutron and X-ray powder diffraction data (Figure 2) with relative weights of 0.8 and 0.2, respectively, based on the relative amount of data for each set. The structure of the mineral paramelaconite (Cu_4O_3) was used as a starting model.[30] In successive cycles, atomic and profile parameters were refined, up to a total of 56, including anisotropic thermal parameters for all atoms and refinement of a small amount (2%) of CuO impurity (detected only in the neutron diffraction data due to difficulties in scaling up the synthesis). Pseudo-Voigt functions were used to fit peak shapes between Lorentzian and Gaussian, and the peak width of the X-ray diffraction pattern was refined with the usual constraints (quadratic polynomial on tan θ) imposed by Caglioti's formula: $\text{fwhm}^2 = U(\tan\theta)^2 + V\tan\theta + W$. In the case of neutron data, it was necessary to consider peak width anisotropy by using spherical harmonic coefficients. The final refinement converged yielding the reliability factors shown in Table 1, which includes crystal and refinement data.

Table 1. Crystallographic Data for $Ag_2Cu_2O_3$

chemical formula	$Ag_2Cu_2O_3$
fw (g/mol)	390.84
space group	$I4_1/amd$
a	5.8862(2) Å
c	10.6892(4) Å
V	370.35 Å^3
Z	4
T	25 °C
λ (X-ray)	1.5418 Å
D_{calcd} (g·cm^{-3})	7.01
R_p, R_{wp}, R_{expn}, χ^2 (neut)[a]	4.00, 4.93, 3.43, 2.07
R_p, R_{wp}, R_{expx}, χ^2 (X-ray)	4.52, 6.10, 2.66, 5.26
global instability index	0.137

[a] $R_p = 100(\sum|Yi_{obsd} - Yi_{calcd}|/\sum|Yi_{obsd}|)$; $R_{wp} = 100[(\sum w|Yi_{obsd} - Yi_{calcd}|^2/\sum w|Yi_{obs}|^2)]^{1/2}$; $R_{exp} = 100[(N - P + C)/\sum w|Yi_{obsd}|^2]^{1/2}$; $\chi^2 = [R_{wp}/R_{exp}]^2$ where N is the number of measured points in the pattern, P is the number of refined parameters, and C is the number of constraint functions.

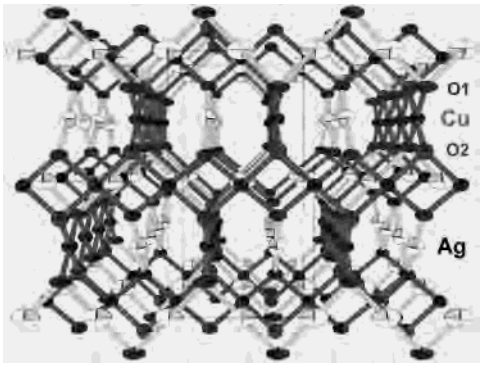

Figure 3. Crystal structure of $Ag_2Cu_2O_3$. Ag^I shown as white ellipsoids, Cu^{II} as black ellipsoids, and oxygen ions as gray ellipsoids. A unit cell is outlined.

Table 2. Positional Parameters, Thermal Factors, and Valence Sums for $Ag_2Cu_2O_3$

atom	Ag	Cu	O1	O2
site	8c	8d	8e	4b
x	0.0000	0.0000	0.0000	0.0000
y	0.0000	0.0000	0.2500	0.2500
z	0.0000	0.5000	0.1366(3)	0.3750
$\beta 11$	0.007(1)	0.0069(7)	0.007(1)	0.007(1)
$\beta 22$	0.019(1)	0.0056(7)	0.013(1)	0.007(1)
$\beta 33$	0.0023(2)	0.0012(1)	0.0009(3)	0.0018(5)
$\beta 12$	0.0	0.0	0.0	0.0
$\beta 13$	0.0	0.0	0.0	0.0
$\beta 23$	−0.0006(7)	0.0006(5)	0.0	0.0
valence sum	0.969(3)	1.950(3)	2.051(5)	1.737(0)

The structure is shown in Figure 3 and consists of alternating chains of edge-sharing square planar CuO_4 units (crisscross chains) and zigzag chains of linearly coordinated silver ions. These chains run parallel to a and b consecutively as we move along the c direction. This structure is related to that of PdO although in $Ag_2Cu_2O_3$ silver is linearly coordinated and the alternation of Cu and Ag leads to a doubling of the unit cell in all three directions of space. Table 2 shows fractional coordinates and anisotropic thermal parameters for each atom, and Table 3 summarizes relevant

(28) Adelsberger, K.; Curda, J.; Vensky, S.; Jansen, M. *J. Solid State Chem.* **2001**, *158*, 82−86.
(29) Curda, J.; Klein, W.; Liu, H.; Jansen, M. *J. Alloys Compd.* **2002**, *338*, 99 (structure redetermination).
(30) O'Keeffe, M.; Bovin, J. O. *Am. Mineral.* **1978**, *63*, 180−185.

Table 3. Selected Interatomic Distances and Bond Angles for $Ag_2Cu_2O_3$

Distance (Å)	
Ag−O1	2.073(2)
Cu−O1	1.906(2)
Cu−O2	1.9877(1)
Ag···Ag	2.9431(1)/3.3871(1)
Cu···Cu	2.9431(1)/3.3871(1)
Cu···Ag	2.9431(1)/3.3871(1)
Bond Angles (deg)	
O1−Ag−O1	180.0(2)
Ag−O1−Ag	90.44(7)
O1−Cu−O1	180.0(8)
O2−Cu−O2	180.00(1)
O1−Cu−O2	100.1(3)/79.9(6)
Cu−O2−Cu	95.530(8)/116.860(8)
Cu−O1−Cu	104.7(4)
Ag−O1−Cu	116.61(7)

bond distances and angles. The coordination of the metals is typical of Cu^{II} and Ag^{I}. The results of bond valence calculations based on bond distances are also included in Table 2 and confirm this oxidation state assignment. Concerning this crystal structure, there are several unique features worth mentioning. First of all, there are two nonequivalent oxygen atoms (O1, bonded to two Cu and two Ag atoms, and O2, bonded to four Cu atoms). The square planar coordination of Cu^{II} suffers a concurrent rhombic distortion with a short Cu−O1 bond and a longer Cu−O2 bond. The Ag−O1 bond in the title oxide (2.073(2) Å) is correspondingly longer than those found in silver oxides with analogous linear coordination (2.02−2.04 Å). The displacement of O1 toward Cu^{II} and away from Ag^{I} is easy to understand from a simple ionic point of view and explains the thermal stabilization of $Ag_2Cu_2O_3$ relative to other silver oxides which was already mentioned.

Electronic Structures of $Ag_2Cu_2O_3$ and Cu_4O_3. To gain some insight into the electronic structure of this material, we have carried out electronic band calculations for $Ag_2Cu_2O_3$ and the related paramelaconite (Cu_4O_3) at two levels of theory (see Experimental Section for details). We use the results of extended Hückel tight binding (EHTB) calculations for the qualitative description of the band structure at the one-electron level. Spin polarized density functional (DFT) band calculations that take into account the two-electron interactions are used to asses the qualitative results and to provide a semiquantiative estimate of the relative energies of the different spin states. The density of states (DOS) curves obtained from the EHTB calculations for the hypothetical nonmagnetic state (Figure 4) clearly indicate that the states in the vicinity of the Fermi level are localized on the Cu^{II} atoms in both compounds. These levels are separated by a gap from the rest of the low-lying occupied metal d bands. The analysis of the atomic orbital contributions to those bands reveals that these levels arise mainly from the $x^2 - y^2$ type orbitals of the Cu^{II} atoms, as should be expected from the local square planar ligand field around them.[31] It is remarkable that the position of these bands is determined solely by the different coordination environment of the mono- and divalent metal ions, because in this very qualitative approach we use the same atomic parameters (ionization potentials and Slater exponents) for Cu^{II} and Cu^{I}. However, it should be borne in mind that consideration of interelectron interactions (not included in the EHTB calculations) of the $x^2 - y^2$ type orbitals with α and β spin will be shifted down and up in energy, respectively, thus opening a gap consistent with the magnetic states. This situation is addressed below (or in following paragraphs) with the help of DFT spin polarized calculations.

(31) Albright, T. A.; Burdett, J. K.; Whangbo, W.-H. *Orbital Interactions in Chemistry*; Wiley: New York, 1985; p 298.

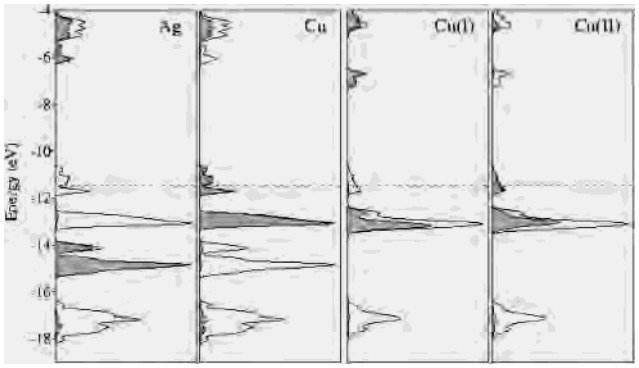

Figure 4. Density of states (DOS) for $Ag_2Cu_2O_3$ (left) and Cu_4O_3 (right) obtained from EHTB calculations. The shaded areas correspond to the contribution of the metal atoms indicated in each panel. The dashed line indicates the position of the Fermi level considering a hypothetical nonmagnetic state.

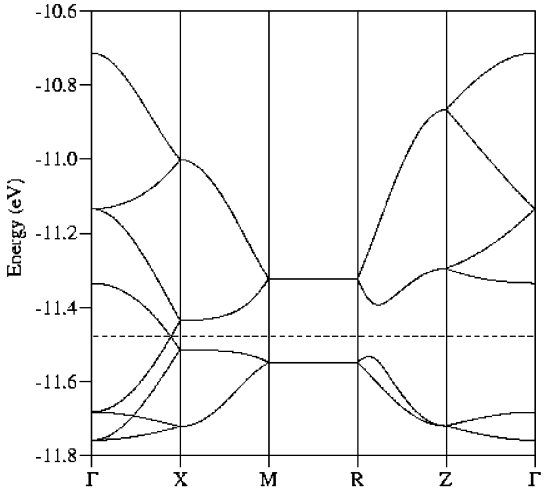

Figure 5. Band structure for $Ag_2Cu_2O_3$ obtained from EHTB calculations. The dashed line indicates the position of the Fermi level corresponding to a hypothetical nonmagnetic state.

The calculated dispersion relationships for these bands along several symmetry lines of the Brillouin zone (BZ) are shown in Figure 5 for $Ag_2Cu_2O_3$. They present bandwidths of around 1 eV along the *a* and *b* chain directions (ΓX direction of the Brillouin zone) and also along the interchain *c* direction (ΓZ direction in the Brillouin zone). Because the bands around the Fermi level are relatively narrow, two-electron terms can lead to an effective localization of the $x^2 - y^2$ electrons that may favor magnetically ordered states over the metallic state predicted from the one-electron band picture. The dispersion diagram for Cu_4O_3 (not shown) is very similar to that of $Ag_2Cu_2O_3$.

Let us discuss now the DFT calculations that allow us to go beyond the qualitative band picture described here and

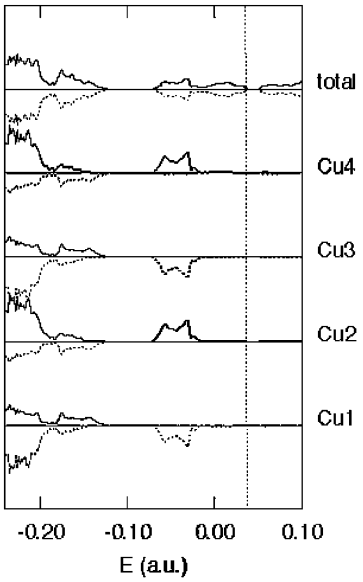

Figure 6. Calculated total density of states (top) and atomic contributions of the Cu atoms to the DOS (×8) for the α (solid line) and β (dashed line) electrons in $Ag_2Cu_2O_3$ using spin polarized density functional calculations. The Fermi level is indicated with a dotted line.

evaluate the relative stability of the different magnetic states expected for such systems with intermediate bandwidths. The general qualitative aspects discussed in a preceding paragraph at the one-electron level are confirmed by these calculations: (i) the bands around the Fermi level are well separated from all other bands and are built up mostly by the Cu^{II} $x^2 - y^2$ orbitals, and (ii) similar bandwidths are found along the lines of the reciprocal space corresponding to the *a* and *c* crystallographic directions. If we consider the structure built up from perpendicular chains of Cu^{II} ions, we can think of ferro- or antiferromagnetic coupling within and between the chains. We have analyzed three possible overall spin states (Scheme 1): F, in which the neighboring spins are ferromagnetically coupled both within and between the chains; A, in which the coupling is ferromagnetic within the chains but antiferromagnetic between chains; and A′, in which the Cu^{II} ions are antiferromagnetically coupled along the chains. The calculated relative energies for such localized states are shown in Scheme 2. We illustrate the results by showing in Figure 6 the spin polarized density of states at the Cu atoms of $Ag_2Cu_2O_3$ in the A′ state. In this case, because of the two-electron interactions, the α $x^2 - y^2$ bands are below the Fermi level for one atom in a chain (Cu2 or Cu4), whereas for the nearest neighbor in a chain (Cu1 or Cu3) it is the β $x^2 - y^2$ bands that are occupied, consistent with the schematic description in Scheme 1.

We make use of a Heisenberg−Dirack−Van Vleck spin Hamiltonian that considers only pairwise interactions between nearest neighbors and disregards next-nearest neighbor interactions:

$$\hat{H} = -J_a\sum_{i,j}\hat{S}_{i,j}\hat{S}_{i+1,j} - J_c\sum_{i,j}\hat{S}_{i,j}\hat{S}_{i,j+1} - J_c\sum_{i,j}\hat{S}_{i,j}\hat{S}_{i+1,j+1} \quad (1)$$

where $\hat{S}_{i,j}$ is the spin operator corresponding to the Cu atom occupying position *i* in chain *j*. Thus, J_a is the coupling constant for the interaction along the chains and J_c for the

Scheme 1

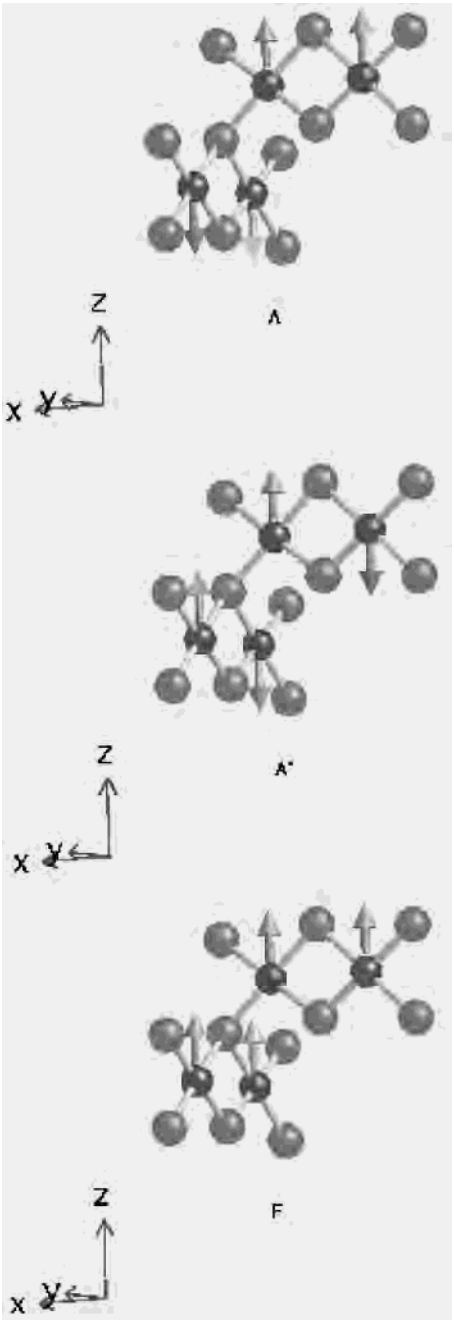

interaction between neighboring perpendicular chains. Energy differences between different spin distributions can be obtained in a simple way by associating pairwise interactions between neighbors to the coupling constants,[32] whereupon the following relationships result:

$$J_c = \frac{E_A - E_F}{16} \quad (2)$$

$$J_a = -\frac{1}{8}\left(\frac{E_A + E_F}{2} - E_{A'}\right) \quad (3)$$

From the energies calculated for the three states, the resulting coupling constants are $J_a = -22.6$ cm^{-1}, $J_c =$

(32) Chartier, A.; D'Arco, P.; Dovesi, R.; Saunders, V. R. *Phys. Rev. B* **1999**, *60*, 14042.

Scheme 2

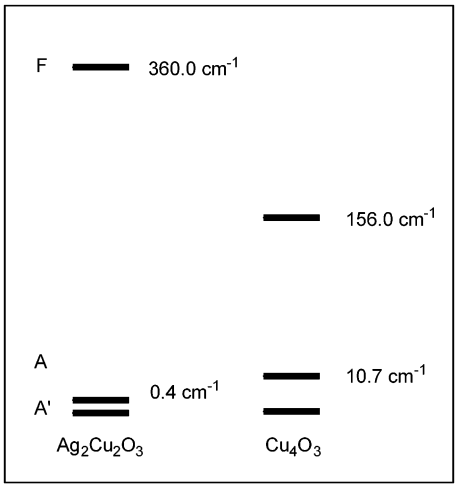

-22.5 cm^{-1} for $Ag_2Cu_2O_3$, and $J_a = -11.1$ cm^{-1}, $J_c = -9.8$ cm^{-1} for Cu_4O_3. These surprisingly close values will be discussed in following paragraphs.

Magnetic Properties of $Ag_2Cu_2O_3$. The thermal variation with temperature of both χ (molar susceptibility) and χT at 10 kG for $Ag_2Cu_2O_3$ are presented in Figure 7. The susceptibility (5.9×10^{-4} cm^3 mol^{-1} at 290 K) increases upon decreasing the temperature, reaching a broad maximum at ca. 80 K, with $\chi = 7.1 \times 10^{-4}$ cm^3 mol^{-1}. Below this temperature, an abrupt drop of the magnetic molar susceptibility is observed, leading to a minimum value of 5.6×10^{-4} at 30 K, followed by an increase at lower temperatures possibly due to minor amounts of paramagnetic impurities. The position of the maximum, together with the continuous decrease in the χT values, is indicative of antiferromagnetic behavior of the compound, which is strong already at room temperature as reflected by the low value of the effective magnetic moment ($\mu_{eff} = 1.2\mu_B$ at room temperature [$\mu_{eff} = 2.83(\chi T)^{1/2}$].

From the crystal structure (Figure 3), one should expect important superexchange interactions through the oxo bridges to arise both along a chain (*a* and *b* crystallographic directions) and between the chains (*c* direction). The interaction through the Ag^I ions are neglected in a first approximation. Although there are no models available for extracting exchange coupling constants from the susceptibility data for three-dimensional systems, a semiquantitative approach can be performed by using a mean field corrected chain model. The molar susceptibility of such a system can be expressed as that of a chain (Y)[33] corrected by taking into account interchain coupling:

$$\chi = \frac{Y}{1 - \dfrac{zJ_cY}{Ng^2\beta^2}} \tag{4}$$

$$Y = \frac{Ng^2\beta^2}{k_BT}\,\frac{A + Bx + Cx^2}{1 + Dx + Ex^2 + Fx^3} \tag{5}$$

where $x = |J_a|/k_BT$, z is the number of interchain nearest neighbors ($z = 2$ in this case), and the coefficients *A*, *B*, *C*, *D*, *E*, and *F* take the values 0.25, 0.14995, 0.30094, 1.9862, 0.68854, and 6.0626, respectively.[33]

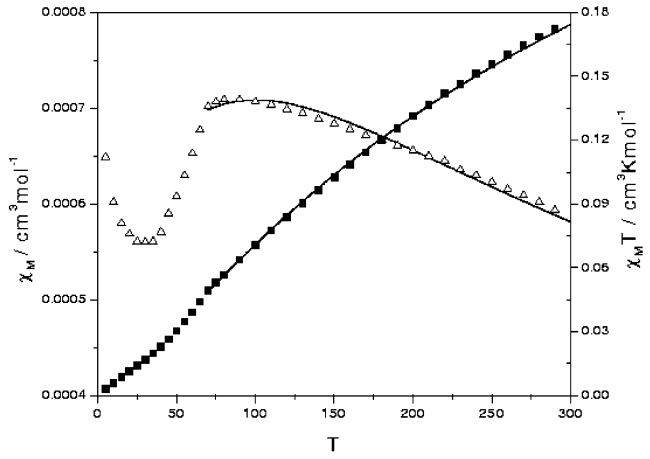

Figure 7. Molar magnetic susceptibility data for $Ag_2Cu_2O_3$ (open triangles) (per copper ion and corrected for diamagnetism) and fit of the data at $T >$ 85 K corresponding to a model with two coupling constants, $J_a = -53.7$ cm^{-1}, $J_c = -22.4$ cm^{-1}.

The best fit of the experimental data to eq 4 was obtained with $J_a = -53.7$ cm^{-1}, $J_c = -22.4$ cm^{-1}, and $g = 2.2$. The agreement factor, defined as $R = (\chi_{calcd} - \chi_{obsd})^2/(\chi_{obsd})^2$, was 5.6×10^{-5} and can be considered as acceptable. In the calculation, only the data obtained above 85 K were used, because these equations are not valid for long range ordered magnetic states, and the drop in the susceptibility below 75 K may correspond to a phase transition or to a long range ordered magnetic state. This is presently being studied by low-temperature neutron diffraction.

Let us now compare the results obtained from fitting the magnetic susceptibility data with those from DFT calculations. We cannot take the exchange coupling constants obtained from the fitting of the high-temperature susceptibility data of $Ag_2Cu_2O_3$ as precise numerical values, given the limitations of the model applied and of the experimental data set used. However, two qualitative conclusions can be drawn: (i) the compound is moderately antiferromagnetic, and (ii) coupling between chains is similar in sign and magnitude to that within the chains. These conclusions are consistent with the *J* values obtained from extended DFT calculations, as well as with the small value of the magnetic moment at room temperature and its decrease upon cooling.

The present compound is related to a family of solid state copper oxides that show edge sharing chains of square planar CuO_4 cores, but it can also be related to the binuclear oxo- or hydroxo-bridged Cu(II) complexes that have been widely studied in the past decades. Among the solid state Cu(II) compounds presenting CuO_2 ribbons we can mention CuO (with a structure derived from that of PtS[34,35]), Li_2CuO_2,[36] and $CuGeO_3$,[37] but similar ribbons can be found in the Cu^{III}

(33) Estes, W. E.; Gavel, D. P.; Hatfield, W. E.; Hodgson, D. J. *Inorg. Chem.* **1978**, *17*, 1415.
(34) Brese, N. E.; O'Keefe, M.; Ramakrishna, B. L.; Dreele, R. B. v. *J. Solid State Chem.* **1990**, *89*, 184.
(35) Massaroti, V.; Capsoni, D.; Bini, M.; Altomare, A.; Moliterni, A. G. G. *Z. Kristallogr.* **1998**, *213*, 259.
(36) Sapiña, F.; Rodríguez-Carvajal, J.; Sanchis, M. J.; Ibáñez, R.; Beltrán, A.; Beltrán, D. *Solid State Commun.* **1990**, *74*, 779.

oxide $NaCuO_2$[38] and in Cu^{II}/Cu^{III} mixed valence oxides such as $Sr_{0.75}CuO_2$[39] or $Ca_{1-x}CuO_2$,[40] and combined with Cu_2O_3 ladders in $(Ca_{1-x}Y_x)_{0.82}CuO_2$.[41] On the molecular side, magnetostructural correlations for hydroxo-bridged binuclear Cu^{II} complexes have been extensively studied in the past decades.[42,43]

From the experimental and theoretical study of such diverse systems, it can be now concluded that the sign and the magnitude of the exchange interaction between neighboring Cu atoms within a ribbon with OX_n bridges is affected by the following factors:[42,44−46] (i) the Cu−O−Cu bond angle θ, (ii) the nature and number of the X groups, and (iii) the position of the X substituent (for $n = 1$) relative to the Cu_2O_2 plane. The exchange coupling constant increases with decreasing θ, eventually reaching positive values (i.e., ferromagnetic coupling). The actual angle for which the crossover from antiferro- to ferromagnetic interaction appears varies with the nature and number of substituents at the bridging oxygens. For a trinuclear model of $CuGeO_3$, in which each oxo bridge is attached to two Ge atoms, ferromagnetism is predicted at $\theta < 98°$,[46] practically the same angle found for hydroxo-bridged binuclear complexes.[42] Substitution of the hydroxo bridges by methoxo ones shifts the antiferromagnetic−ferromagnetic crossover angle to about 95°,[42] but for unsubstituted oxo bridges, the crossover appears at $\theta \approx 108°$.[45] In Cu_4O_3 and $Ag_2Cu_2O_3$, the neighboring Cu^{II} ions in a ribbon are bridged by two different oxygen atoms: one is bonded to two more square planar Cu^{II} ions, the other one, to two linear Cu^{I} (or Ag^{I}) ions. Given the similar electronegativities of Ge, Cu, and Ag, one should expect the crossover angle in this family of compounds to be similar to that of $CuGeO_3$. The calculated J_a values for Cu_4O_3 and $Ag_2Cu_2O_3$, −10.5 and −22.5 cm^{-1}, respectively, are in excellent qualitative agreement with the general trends, given the θ bond angles of 97.5° and 100.1° (average value), respectively.[47] Experimentally, the intraribbon coupling in $CuGeO_3$, with a bond angle of 99.2°, is antiferromagnetic ($-83 > J_a > -125$ cm^{-1}).[48−51] In contrast, a ferromagnetic intraribbon coupling in Li_2CuO_2 ($J_a = 69.5$ cm^{-1} but in a model with a J for next-nearest-neighbors)[52] appears at a quite smaller angle of 94.0°.[36]

The exchange coupling between the Cu^{II} ions in different ribbons present a topology, with a single oxo bridge linking the two perpendicular square planar coordination spheres, that has been less investigated. Our empirical analysis of the magnetic susceptibility above 85 K is consistent with our theoretical study in describing the inter-ribbon interaction as weakly antiferromagnetic. The experimentally derived value for the related Li_2CuO_2 is also weakly antiferromagnetic ($J_c = -11.1$ cm^{-1}).[52] We note also that similar interactions along the *a* and *c* crystal directions are consistent with the calculated band dispersion diagrams (Figure 5) that show similar bandwidths along the corresponding directions of the reciprocal space.

The importance of the exchange interaction between chains is further evidenced by comparing the structure and magnetic behavior of $Ag_2Cu_2O_3$ with those of CuO. In the former, the bridge angle within a chain is $\theta = 100.1°$ (average), while in the latter it is 95.7°. On the basis of the intrachain interaction only, one would expect stronger antiferromagnetism for $Ag_2Cu_2O_3$, in contradiction with the experimental findings, because CuO presents a maximum in its magnetic susceptibility at 550 K,[53] compared with 80 K in the present case. If we consider interaction between neighboring chains, though, one realizes that in CuO two bridging oxo ligands of one chain are simultaneously bridging two approximately perpendicular chains, whereas in $Ag_2Cu_2O_3$ only one of the oxo bridges is shared by perpendicular chains and the other one is linked through two Ag(I) ions to a neighboring chain. Therefore, it seems reasonable to assume that the interchain Cu(II)−O−Cu(II) interaction is more strongly antiferromagnetic than the Cu(II)−O−Ag(I)−O−Cu(II) one.

Let us recall here that we have disregarded the interaction between next-nearest neighbors in our calculations and that the fitting of the high-temperature susceptibility data corresponds to a system with two coupling constants. Hence, it might well be that exchange interactions between next-nearest neighbors in the chains are non-negligible, as found for Li_2CuO_2 experimentally[52] and theoretically[46] for a model of $CuGeO_3$. Therefore, the determination of the magnetic structure by low-temperature neutron diffraction experiments, which is presently under study, is an important step toward the understanding of the exchange interactions in copper(II) oxides formed by nonisolated ribbons.

Transport Properties of $Ag_2Cu_2O_3$. Alternating current impedance measurements were carried out in order to study the electrical behavior of the sample and the contribution of the grain boundary resistance. The pellets were only pressed, as the material cannot be sintered at high temperatures because of its limited thermal stability, and the contacts were made with silver paint. Gold electrodes were used. Several

(37) Braden, M.; Ressouche, E.; Buechner, B.; Kessler, R.; Heger, G.; Dhalenne, G.; Revcolebschi, A. *Phys. Rev. B* **1998**, *57*, 11497.
(38) Hestermann, K.; Hoppe, R. *Z. Anorg. Allg. Chem.* **1969**, *367*, 261.
(39) Karpinski, J.; Schwer, H.; Meijer, G. I.; Conder, K.; Kopnin, E. M.; Rossel, C. *Phys. C (Amsterdam)* **1997**, *274*, 99.
(40) Siegrist, T.; Roth, R. S.; Rawn, C. J.; Ritter, J. J. *Chem. Mater.* **1990**, *2*, 192.
(41) Miyazaki, Y.; Hyatt, N. C.; Slaski, M.; Gameson, I.; Edwards, P. P. *Chem. Eur. J.* **1999**, *5*, 2265.
(42) Ruiz, E.; Alemany, P.; Alvarez, S.; Cano, J. *J. Am. Chem. Soc.* **1997**, *119*, 1297.
(43) Crawford, W. H.; Richardson, H. W.; Wasson, J. R.; Hodgson, D. J.; Hatfield, W. E. *Inorg. Chem.* **1976**, *15*, 2107.
(44) Ruiz, E.; Alemany, P.; Alvarez, S.; Cano, J. *Inorg. Chem.* **1997**, *36*, 3683.
(45) Ruiz, E.; Alvarez, S.; Alemany, P. *Chem. Commun.* **1998**, 2767.
(46) Ruiz, E.; Cano, J.; Alvarez, S.; Alemany, P.; Verdaguer, M. *Phys. Rev. B* **2000**, *61*, 54.
(47) It has been computationally shown that the *J* value in asymmetric binuclear hydroxo-bridged complexes is more negative for the same average angle as the asymmetry increases: Ruiz, E.; Alemany, P.; Alvarez, S.; Cano, J. *Inorg. Chem.* **1997**, *36*, 3683.
(48) Nojiri, H.; Shmamoto, Y.; Miura, N.; Hase, M.; Uchinokura, K.; Kojima, H.; Tanaka, I.; Shibuya, Y. *Phys. Rev. B* **1995**, *52*, 12749.
(49) Castilla, G.; Chakravarty, S.; Emery, V. J. *Phys. Rev. Lett.* **1995**, *75*, 1823.
(50) Riera, J.; Dobry, A. *Phys. Rev. B* **1995**, *51*, 16098.
(51) Fabricius, K.; Lümper, A.; Löw, U.; Büchner, B.; Lorenz, G.; Dhalenne, G.; Revcolevschi, A. A. *Phys. Rev. B* **1998**, *57*, 1102.
(52) Mizuno, Y.; Tohyama, T.; Maekawa, S. *Phys. Rev. B* **1999**, *60*.
(53) Hodge, I. M.; Ingram, M. D.; West, A. R. *J. Electroanal. Chem.* **1976**, *74*, 125−143.

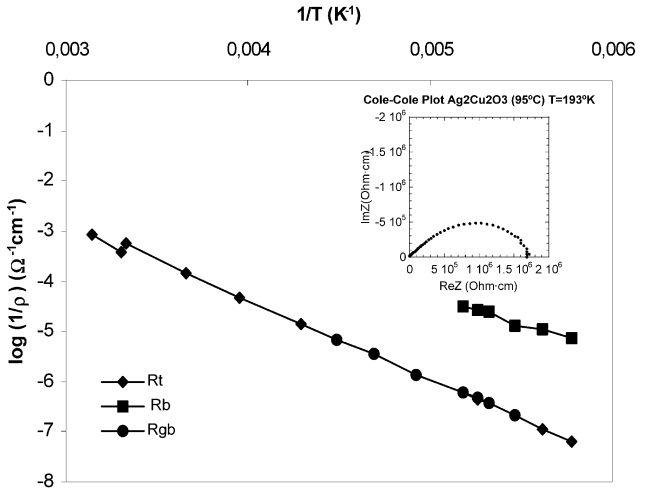

Figure 8. Arrhenius plot of the total, intergrain, and intragrain conductivity of $Ag_2Cu_2O_3$. In the inset, a Cole−Cole plot at 193 K is shown.

samples were measured showing no apparent difference in their results. A typical set of AC data, in the form of a complex impedance plane plot (Cole−Cole plot), is given in the inset of Figure 8. This plot allows us to distinguish between the electrical conductivity assigned to the intragrain (or bulk) and intergrain (or grain boundary) processes, taking advantage of the fact that each one dominates at different frequencies and resulting in separate semicircles for each kind of conduction (for a more detailed description, see refs 53 and 54). It is difficult to distinguish the two semicircles, which appear more clearly in the modulus plot. The low-frequency semicircle can be assigned to the grain boundary while the high-frequency one, which passes through the origin, was associated with the intragrain or bulk response of the sample. The values of their capacitance, $C_{gb} = 10-40$ pF (grain boundary) and $C_b = 1-4$ pF (bulk), found from the maximum of each semicircle, using the relation $\omega RC = 1$, are consistent with this assignment.[54] The total resistance of the sample is determined predominantly by the grain boundary factor. For any given sample, the slope of the Arrehnius plot (Figure 8) for both processes is the same within experimental error. This implies a similarity in the activation energy of R_{gb} (resistance of grain boundary) and R_b (resistance of bulk). Both the relatively small capacitance values of C_{gb} and the similarity in grain boundary and bulk activation energies have been previously reported in certain LISICON phases.[55] This atypical behavior has been interpreted through the presence of constricted pathways for current flow due to air gaps typically present in unsintered polycrystalline samples or in materials with effective densities much lower than their theoretical values.[55]

The moderate conductivity found experimentally (within the range of semiconducting materials) can be consistent with our present calculations showing essential electron localization if we consider the presence of point defects and a hopping mechanism similar to what happens for CuO.[56]

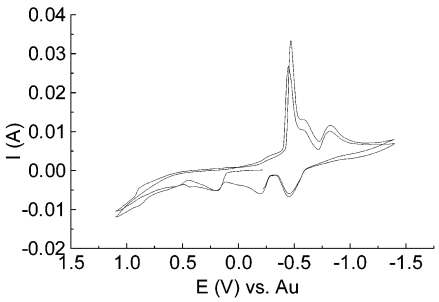

Figure 9. Cyclic voltammetry of $Ag_2Cu_2O_3$. The second and third cycles are shown.

Electrochemical Characterization of $Ag_2Cu_2O_3$. The remarkable structure of $Ag_2Cu_2O_3$ presents a three-dimensional array of tunnels (parallel to *a* and *b*) with a minimum dimension corresponding to the Ag···Cu separation of 2.9431(1) Å (*a*/2). As in $YBa_2Cu_3O_6$, these metal-constrained tunnels could be most adequate for the diffusion of oxygen species. The tunnels lead directly to vacant oxygen sites that could be occupied with the concomitant oxidation of Ag^I (linear coordination) to Ag^{III} (square planar). Also, in principle, the structure could easily stand the elimination of one oxygen atom (O2) with the simultaneous reduction of Cu^{II} (square planar) to Cu^I (linear). To study these possibilities, we carried out a detailed electrochemical characterization of this new oxide. Figure 9 shows the second and third cyclic voltammograms of a pressed pellet of $Ag_2Cu_2O_3$.

To identify the products of each redox reaction, chronoamperometries were carried out at potential values of each electrochemical process, and the phases obtained were characterized by X-ray diffraction. In this way, we are able to unambiguously assign every wave to the corresponding redox process. The first reduction observed at −0.45 V versus Au corresponds to the reduction of Ag(I) ions in $Ag_2Cu_2O_3$ to yield metallic Ag, segregation of CuO, and the consequent decomposition of the phase. The second (−0.59 V vs Au) and third (−0.82 V vs Au) waves correspond to the reduction of CuO to cuprite and to metallic copper, respectively. These results explain why during the first oxidation cycle no major oxidation wave was observed (with the exception of a weaker wave at 0.57 V vs Au discussed later). After the first cycle, three major oxidation waves (at −0.45, −0.20, and 0.18 V, respectively) can be clearly observed which are assigned to the inverse redox processes, from Cu^0 to Cu(I) and Cu(II) and Ag^0 to Ag(I). Nevertheless, the reductive decomposition of $Ag_2Cu_2O_3$ leads to the eventual formation of Ag_2O and CuO as final oxidation products.

Aside from that, there is an additional less sharp wave at 0.57 V (also detected in the first oxidation cycle) corresponding to the oxidation of $Ag_2Cu_2O_3$ which has been shown to lead to a novel oxidized phase, $Ag_2Cu_2O_4$.[57] The nature and structure of this phase, which has also been obtained chemically,[58] is still under investigation.

(54) Irvine, J. T. S.; Sinclair, D. C.; West, A. R. *Adv. Mater.* **1990**, *2*, 132−138.
(55) Bruce, P. G.; West, A. R. *J. Electrochem. Soc.* **1983**, *130*, 662−669.
(56) *GMELIN'S Handbuch der Anorganischen Chemie*; Verlag Chemie: Berlin, Kupfer, 1963; Vol. 60D, p 84.
(57) (a) Muñoz-Rojas, D.; Tejada-Rosales, E. M.; Gómez-Romero, P.; Casañ-Pastor, N. *Bol. Soc. Esp. Ceram. Vidrio* **2002**, *41*, 55. (b) Muñoz-Rojas, D.; Oro, J.; Gómez-Romero, P.; Fraxedas, J.; Casañ-Pastor, N. *Electrochem. Commun.* **2002**, *4*, 684.

Conclusions

The synthesis of $Ag_2Cu_2O_3$ was first undertaken in an attempt to explore low-temperature pathways for the preparation of hitherto unknown mixed silver copper oxides. The successful isolation and structural characterization of the title compound showed a simple synthetic route to complex silver oxides which could likely expand the number of known phases of this kind, as has been later confirmed by the isolation of another silver copper phase, $Ag_5(Pb,Cu)_2O_6$,[7] also synthesized by means of the use of the same synthetic route.

In addition to the synthetic interest, the crystal structure of the phase reported here has uncovered a network of silver(I) and magnetic copper(II) ions which constitute a unique framework for three-dimensional magnetic interactions of $S = {}^1/_2$ ions. The similar magnitudes of intra- and interchain couplings found in the present work point out the possibility of a magnetically frustrated system which should merit further studies. Finally, the increased thermal stability of the title oxide and its chemical relationship with simple silver oxides induced us to carry out studies of their catalytic properties that have recently led to very positive results concerning partial oxidation reactions.[59]

Thus, the title oxide sets an important precedent in fundamental aspects related to inorganic chemistry and superconducting-related materials. But it also represents new uncharted territory in mineral chemistry, and in applied fields that range from electrochemistry[57] to catalysis[59] and magnetism.[60]

Acknowledgment. This work was funded by CICYT (Spain) (MAT2002-04529-C03 and PB98-1166-C02-01). We also thank the Ministry of Education and Culture (Spain) for a predoctoral fellowship awarded to E.M.T.-R. The authors are also grateful to Dr. F. D. Morrison and Prof. A. R. West for complex impedance measurements, and to Dr. P. Espinós and Dr. J. Fraxedas for XPS measurements.

Supporting Information Available: Crystallographic data and results from combined X-ray/neutron refinement in CIF format. This material is available free of charge via the Internet at http://pubs.acs.org.

IC025872B

(58) Curda, J.; Klein, W.; Jansen, M. *J. Solid State Chem.* **2001**, *162*, 220−224.

(59) Gómez-Romero, P.; Tejada-Rosales, E. M.; Muñoz-Rojas, D.; Casañ-Pastor, N.; Mestl, G.; Wölk, H.-J. Patent 200,201,309, Spain, June 6, 2002.

(60) A very recent report by Whangbo and Koo dealing with theoretical studies of Cu_4O_3 and $Ag_2Cu_2O_3$ supports the interest of this phase from the magnetic point of view: Whangbo, M.-H.; Koo, H.-J. *Inorg. Chem.* **2002**, *41*, 3570.